Analysis of Samara-Wing Decelerator Steady-State Characteristics

Peter Crimi*
Textron Defense Systems, Wilmington, Massachusetts

A method has been developed for computing the steady-state descent characteristics of a samara-wing decelerator. The system is modeled with 11 degrees of freedom taken into account. Analytic requirements for steady vertical descent in lunar rotation derived from the equations of motion are imposed by iteratively varying the dependent variables defining steady descent. Solutions obtained are in good agreement with test data for configurations weighing 1.5–17 lb.

Introduction

THE effectiveness of a sensor-fused submunition relies on a regular, periodic scanning motion imparted to the submunition during its descent to the target area. A device termed a samara-wing† decelerator can provide this type of motion by causing lunar rotation as well as a steady descent rate of the payload. The wing, which is analogous in its function to the wing of a maple seed, is a rectangular piece of fabric attached at its root to the top of the submunition and formed into an aerodynamic surface by the centrifugal load on a small weight in the tip of the wing.

The function of the device has been demonstrated and quantified by tests in a vertical wind tunnel for several different payload and wing configurations.[1-3] A previous analysis of a samara-wing decelerator is reported by Kline and Koenig,[3] in which an aeroballistic simulation computer program was employed using empirically derived aerodynamic coefficients.

In a more recent study,[4] an analytic model of a submunition employing a samara wing was developed with wing aerodynamic loading computed using a strip assumption. Seven degrees of freedom, including wing flapping response, were modeled. Results of simulations were in good agreement with wind-tunnel measurements, but the model was not suitable for design purposes, because wing torsional response was not represented. Solutions must be obtained by adjusting the amount of blade twist to match the computed and measured descent rates.

In the analysis described here, the conditions in steady descent are determined by iteratively solving the equations of motion for those values of the dependent variables producing a steady vertical descent with lunar rotation. Blade response in both flapping and torsion are realistically taken into account. This method, which avoids the many difficulties of direct simulation of a complex aeroelastic system, evolved from efforts to generalize the previously developed simulation model described in Ref. 4. In so doing, the blade was represented by a set of four elastic cords connecting the tip mass to the submunition. This results in 11 equations of motion for the centerbody and tip mass, 1 rotational degree of freedom of the tip mass being extraneous.

Realistic results were obtained from simulations using this model, but large amounts of computer time were used in order to reach steady-state conditions for a given case. Various attempts to make this simulation model a practical analysis tool led finally to iteratively solving the equations of motion for the steady-state values of the dependent variables. The specific formulations used and results of computations are presented in what follows.

Received Nov. 20, 1986; revision received June 17, 1987.

*Principal Scientist. Member AIAA.

†Samara is a generic term for a winged fruit, such as a maple or ash seed.

Analysis Formulations

Equations of Motion

The system analyzed consists of a cylindrical centerbody and a rod-shaped tip mass connected by four elastic cords, as sketched in Fig. 1. The diagonal cords restrain deformations in the plane of the wing. The other two cords define the leading and trailing edges of the wing. Half of the wing fabric mass is added to the tip mass to account for inertial loading on the wing itself. Body-fixed coordinate systems (x_1, y_1, z_1) and (x_2, y_2, z_2) have their origins at the mass centers of the centerbody and tip mass, respectively, as indicated in Fig. 1. Angular displacement of either body is measured by Euler angles referred to inertial coordinates (X, Y, Z), as defined in Fig. 2. Note that in steady lunar rotation, the Euler angle θ_1 between the centerbody axis and the Z axis, termed the cone angle, is constant, while the rate of change of ψ_1, which is the precession rate, is constant and equal to the magnitude of the angular velocity (the spin rate); ϕ_1 is also constant with a value that generally results in the wing extending radially outward from the Z axis, as indicated in Fig. 2.

To formulate the equations of motion, let ω_{xi}, ω_{yi}, and ω_{zi} denote the body-fixed angular velocity components of the two bodies. Angular momentum components h_{xi}, h_{yi}, and h_{zi} are then given in terms of the moments of inertia and

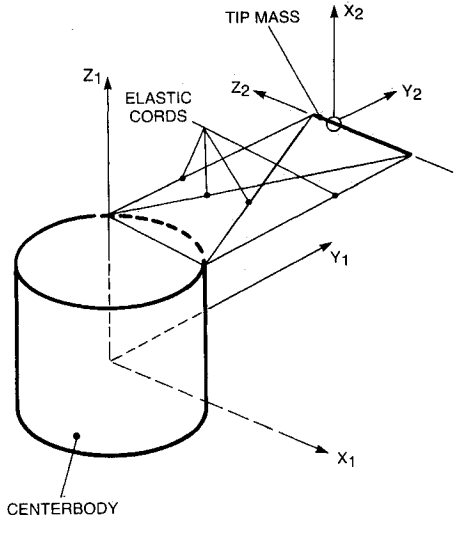

Fig. 1 System analyzed.

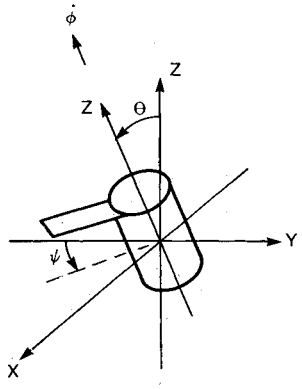

Fig. 2 Euler angle definitions.

angular velocity components by (omitting subscripts i)

$$h_x = I_{xx}\omega_x + I_{xy}\omega_y + I_{xz}\omega_z$$

$$h_y = I_{xy}\omega_x + I_{yy}\omega_y + I_{yz}\omega_z$$

$$h_z = I_{xz}\omega_x + I_{yz}\omega_y + I_{zz}\omega_z$$

The equations of motion for the centerbody are then

$$\dot{h}_{x1} = \omega_{z1}h_{y1} - \omega_{y1}h_{z1} + M_{x1} \tag{1}$$

$$\dot{h}_{y1} = \omega_{x1}h_{z1} - \omega_{z1}h_{x1} + M_{y1} \tag{2}$$

$$\dot{h}_{z1} = \omega_{y1}h_{z1} - \omega_{x1}h_{y1} + M_{z1} \tag{3}$$

$$m_1\ddot{X}_1 = F_{X1} \tag{4}$$

$$m_1\ddot{Y}_1 = F_{Y1} \tag{5}$$

$$m_1\ddot{Z}_1 = F_{Z1} \tag{6}$$

where M_{x1}, M_{y1}, and M_{z1} are the moment components referred to body-fixed axes exerted by aerodynamic loads and cord tensile forces, F_{X1}, F_{Y1}, and F_{Z1} are force components in the inertial frame, and m_1 the centerbody mass.

It is assumed the tip mass, with mass m_2, is attached to the wing in such a way that there is no moment exerted about the z_2 axis and z_2 is a principal axis, with the result that the angular momentum component in the z_2 direction is constant and uncoupled from the other equations of motion and so can be ignored. The remaining tip mass equations are then given by

$$I_{x2x2}\dot{\omega}_{x2} = M_{x2} \tag{7}$$

$$I_{y2y2}\dot{\omega}_{y2} = M_{y2} \tag{8}$$

$$m_2\ddot{X}_2 = F_{X2} \tag{9}$$

$$m_2\ddot{Y}_2 = F_{Y2} \tag{10}$$

$$m_2\ddot{Z}_2 = F_{Z2} \tag{11}$$

Force and Moment Evaluations

The contributions to the force and moment components from the elastic cords are evaluated by calculating the strain in each chord, given the relative positions of the two bodies. The resulting tensile forces exerted at the cord attachment points are calculated from an assumed value for cord stiffness of 10^4 lb/ft.

The aerodynamic loading on the centerbody is computed using coefficients extracted from applicable test data.[5,6] The axial and normal force coefficients obtained are shown in Fig. 3.

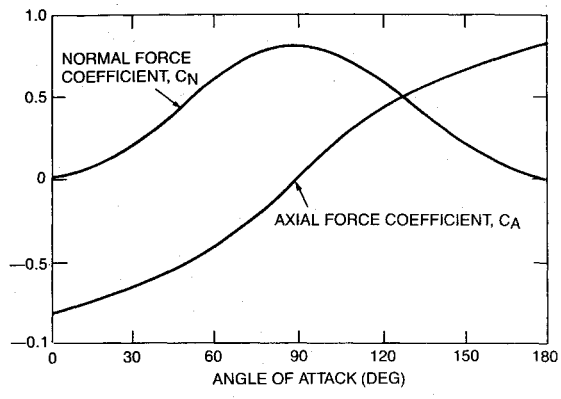

Fig. 3 Centerbody aerodynamic coefficients.

To compute the loading on the samara wing, the flapping angle β, measured from a plane parallel to the x_1-y_1 plane, and the wing twist τ at the tip, positive leading edge up, are calculated from the position and orientation of the tip mass relative to the centerbody. The loading is calculated using a strip assumption, with total load computed by integrating spanwise. The blade section lift ℓ and drag d per unit span are evaluated from the quantities indicated in the sketch of a blade section in Fig. 4. If η is a spanwise coordinate with origin at the blade root, the components of relative fluid velocity at a blade section are given by

$$V_t = -U_0 + \omega_{z1}(y_{1w} + \eta) - \omega_{y1}z_{1w}$$

$$V_n = V_0 \sin\beta - W_0 \cos\beta - w_i - \omega_{x1}(y_{1w} + \eta)$$

where U_0, V_0, and W_0 are the body-fixed components of centerbody velocity, y_{1w} and z_{1w} the wing attachment coordinates, and w_i the wake-induced in-flow. Generally, the wing is operating as a helicopter rotor in the so-called windmill-brake state. In that case, the in-flow can be obtained in terms of the rotor thrust T, using momentum considerations, with the result that[7]

$$w_i = -\frac{W_0}{2} - \left[\left(\frac{W_0}{2}\right)^2 - \frac{T}{2\pi\rho(y_{1w}+S)^2}\right]^{1/2}$$

where S is the wing span. Given V_t, V_n, and twist τ at the tip, the local angle of attack α is given by

$$\alpha = \eta\tau/S + \tan^{-1}(V_n/V_t)$$

With section lift and drag coefficients C_ℓ and C_d defined as functions of α, the lift ℓ and drag d per unit span are then

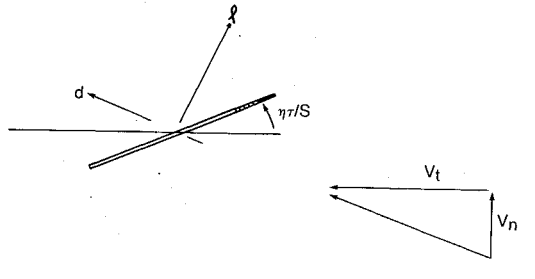

Fig. 4 Relative flow and loading at a wing section.

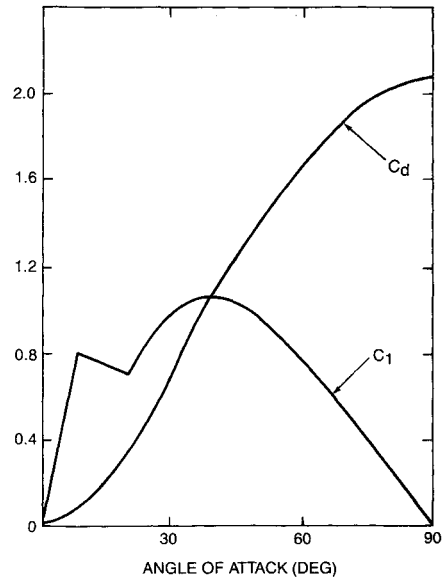

Fig. 5 Wing section lift and drag coefficients.

computed from

$$\ell = \frac{\rho}{2}(V_n^2 + V_t^2)C_\ell(\alpha)$$

$$d = \frac{\rho}{2}(V_n^2 + V_t^2)C_d(\alpha)$$

The variations of C_ℓ and C_d with α were taken from wind-tunnel measurements of an NACA 0012 airfoil section at incidence angles of 0–180 deg.[8] Since the samara wing has a sharp leading edge, the measured data were shifted 180 deg in angle of attack, making the samara-wing stall characteristics the same as those of an airfoil in reversed flow. The section coefficients used are plotted in Fig. 5.

Methods of Solution

For given centerbody and tip mass geometries and inertial properties, the steady-state descent characteristics are obtained by iteratively varying the dependent variables to satisfy the equations of motion. That is, the dependent variables of the physical system become the independent variables of the iteration process. In order to identify an appropriate set of variables, the conditions for steady descent must be imposed analytically. For this purpose, consider the relations between the time derivatives of the centerbody Euler angles and the angular velocity components, given by

$$\dot{\psi}_1 = (\omega_{x1}\sin\phi_1 + \omega_{y1}\cos\phi_1)/\sin\theta_1$$

$$\dot{\phi}_1 = \omega_{z1} - (\omega_{x1}\sin\phi_1 + \omega_{y1}\cos\phi_1)\cot\theta_1$$

$$\dot{\theta}_1 = \omega_{x1}\cos\phi_1 - \omega_{y1}\sin\phi_1$$

With steady lunar rotation, both $\dot{\phi}_1$ and $\dot{\theta}_1$ are zero and $\dot{\psi}_1$ is constant. Thus, it must be that

$$\phi_1 = \tan^{-1}(\omega_{x1}/\omega_{y1}) \tag{12}$$

$$\theta_1 = \tan^{-1}[(\omega_{x1}\sin\phi_1 + \omega_{y1}\cos\phi_1)/\omega_{z1}] \tag{13}$$

$$\dot{\psi}_1 = \omega_{z1}\sec\theta_1 \tag{14}$$

Therefore, specifying ω_{x1}, ω_{y1}, and ω_{z1} completely defines the angular motion of the centerbody in lunar rotation. To define the translational motion of the centerbody mass center, it is necessary to specify the location of the center of rotation. The angular velocity vector is directed vertically in steady lunar rotation, so two inertial coordinates X_{CR} and Y_{CR} locate the center of rotation. Since the components of aerodynamic forces in the horizontal direction are small compared to the weight of the centerbody, the center of rotation will be only slightly displaced from the center of mass of the combined centerbody and tip mass. For purposes of the analysis, it is convenient to locate the center of rotation relative to that mass center, according to

$$X_{CR} = X_{CG} + \delta X$$

$$Y_{CR} = Y_{CG} + \delta Y$$

From Eqs. (12) and (13), the center of rotation has centerbody-fixed coordinates given by

$$x_{1CR} = x_{CG} + \cos\phi_1\delta X + \sin\phi_1\cos\theta_1\delta Y$$

$$y_{1CR} = y_{CG} - \sin\phi_1\delta X + \cos\phi_1\cos\theta_1\delta Y$$

$$z_{1CR} = z_{CG} - \sin\theta_1\delta Y$$

in which

$$(x_{CG}, y_{CG}, z_{CG}) = \frac{m_2}{(m_1+m_2)}(x_{1t}, y_{1t}, z_{1t})$$

where x_{1t}, y_{1t}, and z_{1t} are the centerbody coordinates of the tip mass. Specification of δX, δY, and the descent rate $-\dot{Z}_1$, together with the three angular velocity components, completes the definition of centerbody motion.

The tip mass orientation and position relative to the centerbody define its motion. With the roll orientation of the tip mass left unspecified, this requires five variables—tip mass relative center-of-gravity coordinates x_{1t}, y_{1t}, and z_{1t} and Euler angles ψ_2 and θ_2.

In summary, 11 variables completely define the steady descent characteristics. These are three centerbody angular velocity components, two displacement components of the center of rotation, three relative coordinates of the tip mass, and two tip mass Euler angles. From the equations of motion, the 11 requirements to be satisfied are that $\dot{h}_{x1}$, $\dot{h}_{y1}$, $\dot{h}_{z1}$, $\ddot{Z}_1$, $\dot{\omega}_{x2}$, $\dot{\omega}_{y2}$, and $\dot{\omega}_{z2}$ all equal zero, while $\ddot{X}_1$, $\ddot{Y}_1$, $\ddot{X}_2$, and $\ddot{Y}_2$ equal the appropriate components of centripetal acceleration produced by the prescribed angular motion. During the iteration, the acceleration components are computed in body-fixed coordinates and then transformed to the inertial frame. The body-fixed components for the tip mass are given by

$$a_{Tx1} = \omega_{y1}[\omega_{x1}(y_{1t} - y_{1CR}) - \omega_{y1}(x_{1t} - x_{1CR})]$$
$$- \omega_{z1}[\omega_{z1}(x_{1t} - x_{1CR}) - \omega_{x1}(Z_{1t} - Z_{1CR})]$$

and similarly for a_{Ty1} and a_{Tz1} by cyclic variation of subscripts. The corresponding components a_{CBx1}, a_{CBy1}, and a_{CBz1} for the centerbody are computed by simply replacing x_{1t}, y_{1t}, and z_{1t} by zeros in the expression for the tip-mass acceleration components.

The iterative procedure used can be described analytically as follows. First, denote the 11 variables of the iteration by q_i, $i = 1, 2, \ldots, 11$, where

$$q_1 = \omega_{x1} \quad q_5 = x_{1t} \quad q_9 = \theta_2$$

$$q_2 = \omega_y \quad q_6 = y_{1t} \quad q_{10} = \delta X$$

$$q_3 = \omega_{z1} \quad q_7 = z_{1t} \quad q_{11} = \delta Y$$

$$q_4 = \dot{Z}_1 \quad q_8 = \psi_2$$

Next, denote the functions which are to vanish by $G_i(q_1,q_2,\ldots, q_{11})$, $i = 1, 2,\ldots,11$, where

$$G_1 = \omega_{z1}h_{y1} - \omega_{y1}h_{z1} + M_{z1}$$

$$G_2 = \omega_{x1}h_{z1} - \omega_{z1}h_{x1} + M_{y1}$$

$$G_3 = \omega_{y1}h_{x1} - \omega_{x1}h_{y1} + M_{z1}$$

$$G_4 = F_{Z1}$$

$$G_5 = M_{x2}$$

$$G_6 = M_{y2}$$

$$G_7 = F_{X2} - m_2 A_{TX2}$$

$$G_8 = F_{Y2} - m_2 A_{TY2}$$

$$G_9 = F_{Z2}$$

$$G_{10} = F_{X1} - m_1 A_{CBX1}$$

$$G_{11} = F_{Y1} - m_1 A_{CBY1}$$

where A_{TX2}, A_{CBX1}, etc., are the components of centripetal acceleration in the inertial frame.

The requirements for steady descent can then be written as

$$G_i(q_1,q_2,\ldots,q_{11}) = 0, \qquad i = 1, 2,\ldots,11 \qquad (15)$$

Now, let q_i^k be a value of q_i near the value for steady descent. For convenience of notation, further let

$$G_{ik} = G_i(q_1^k, q_2^k,\ldots,q_{11}^k)$$

$$\left(\frac{\partial G_i}{\partial q_j}\right)_k = \frac{\partial G_i}{\partial q_j^k}(q_1^k,q_2^k,\ldots,q_{11}^k)$$

If q_j^{k+1} is the steady-state value of q_j, each of G_i can be expanded in a Taylor series to give

$$G_{i,k+1} = 0 \approx G_{ik} + \sum_{j=1}^{11}\left(\frac{\partial G_i}{\partial q_j}\right)_k (q_j^{k+1} - q_j^k), \quad i = 1,2,\ldots,11$$

This provides a set of linear algebraic equations to be solved for the $(k+1)$th estimate for the solution

$$\sum_{j=1}^{11} C_{ij}^k q_j^{k+1} = b_i^k, \quad i = 1,2,\ldots,11 \qquad (16)$$

where

$$C_{ij}^k = \left(\frac{\partial G_i}{\partial q_j}\right)_k$$

$$b_i^k = \sum_{j=i}^{11} C_{ij}^k q_j^k - G_{ik}$$

Equations (16) were used to iteratively solve for the values of the dependent variables in steady descent. The partial derivatives are evaluated numerically, according to

$$\frac{\partial G_i}{\partial q_j} \approx [G_i(q_1,q_2,\ldots,q_j+\epsilon,\ldots)$$

$$-G_i(q_1,q_2,\ldots,q_j-\epsilon,\ldots)]/2\epsilon$$

where ϵ is a small number, the appropriate value of which was found by experimentation. Convergence to the solution is very rapid, provided the initial estimates for the q_j are sufficiently close to those of the solution vector. In the absence of a good estimate of the solution, divergence of the iteration is prevented by taking a weighted average of q_j^k and q_j^{k+1} in place of q_j^{k+1} for each succeeding step. When the change between succeeding steps falls below a specified threshold, the value of q_j^{k+1} is used directly.

Results of Computations

The steady-state descent characteristics were computed for each of four different configurations that had been tested in vertical wind tunnels. Test results are reported in Refs. 1 and 2. Samara-wing parameters were varied for each configuration and the results compared with test data. The model parameters for the four configurations are listed in Table 1.

Results for the smallest model, which weighed 1.5 lb, are given in Figs. 6 and 7, with sink rate, spin rate, and cone angle plotted vs the location of the tip-mass center of gravity. The computed spin rates are seen to be in very good agreement with measured values, while the sink rate and cone angle show differences of about 10–15%. The observed sharp drop-off in cone angle and the increase in sink rate with aft c.g. movement are well reproduced.

The best overall agreement between analysis and test was obtained for the 5 lb models. These results are shown in Figs. 8–11, with descent parameters plotted against both span and tip mass. Except for two rather anomolous measured cone angle values (one in Fig. 8 and the other in Fig. 10), the computations match all of the data quite well, both in magnitude and in type of variation with span and tip mass.

Results for the 8 lb model are compared in Figs. 12 and 13, which show the computed variations of descent parameters with tip mass c.g. location for the two wing configurations tested. While the comparison in each case is against a single data point, the agreement is seen to be fairly good, particularly for the larger span (Fig. 12). The greatest percentage difference is in spin rate for the shorter span, with 12 Hz measured and 18 Hz computed. It should be noted that those data were obtained under adverse conditions that may have affected their accuracy. The models were hand-launched into the test section at very low spin rate, due to their large inertias, which caused difficulties in controlling the tunnel speed to achieve an approximation to steady descent conditions.

Similar difficulties were encountered for the 17 lb model, the data points for which are compared with analysis results in Fig. 14. The computed variations with tip mass c.g. location are again shown. Despite the problem in achieving steady state, as indicated by the variation in measured descent rate when the film data were taken, the agreement between analysis and test is quite good.

Table 1 Model parameters of configurations analyzed

Model parameter	Parameter values			
Centerbody				
m_1, lbm	1.54	4.63	7.69	17.3
Diameter, in.	2.5	5.0	5.0	5.78
Height, in.	2.65	4.32	3.6	4.93
I_{x1}, I_{y1}, lb·in.^{2}	1.55	15.5	21.3	62.4
I_{z1}, lb·in.^{2}	1.60	18.3	28.2	72.2
Samara wing				
Span, in.	Varied	Varied	7.5, 10.0	14.0
Chord, in.	2.0	4.0	4.0	4.0
m_2, lbm	0.075	Varied	0.105, 0.195	0.173
Tip mass c.g., % chord	Varied	25	25	26

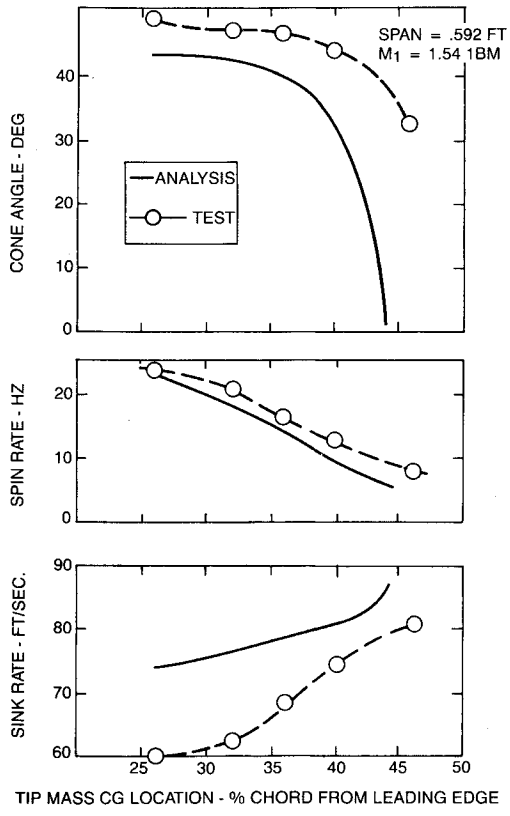

Fig. 6 Comparison of analysis and test, 1.5 lb model, 7.1 in. span.

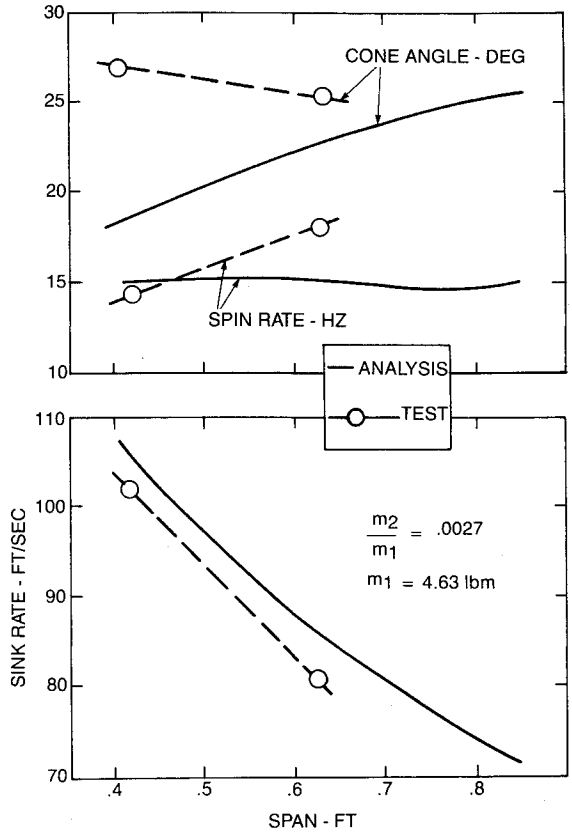

Fig. 8 Comparison of analysis and test, 5 lb model, 2.3% tip mass.

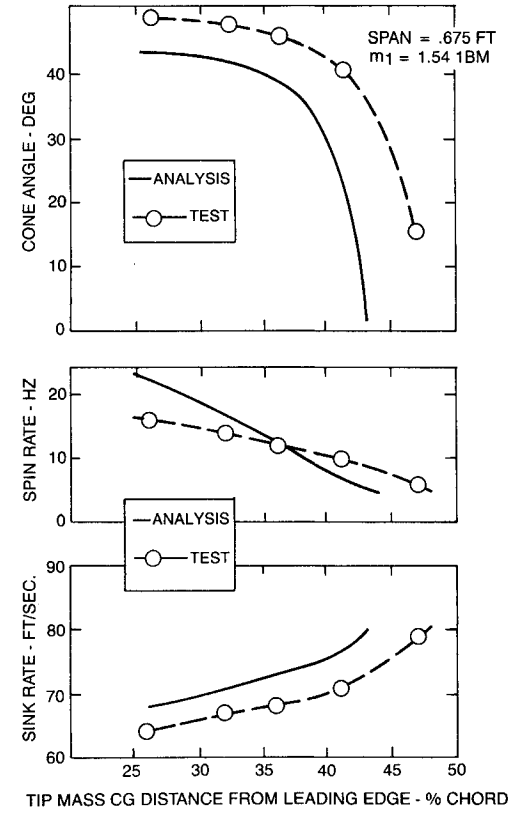

Fig. 7 Comparison of analysis and test, 1.5 lb model, 8.1 in. span.

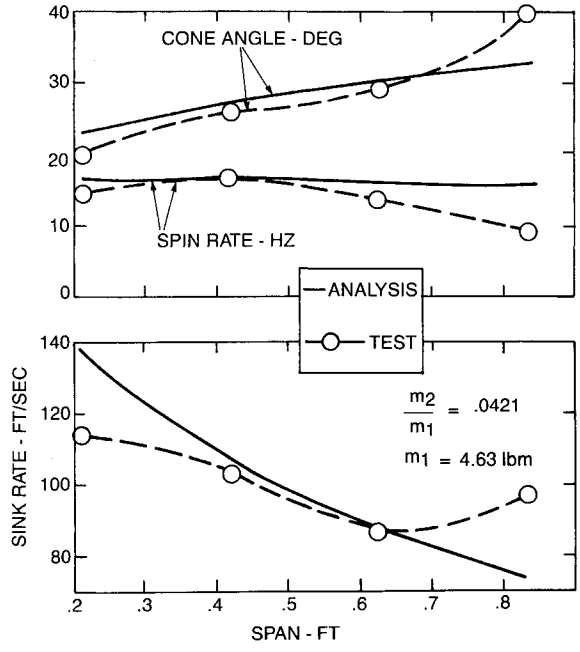

Fig. 9 Comparison of analysis and test, 5 lb model, 4.2% tip mass.

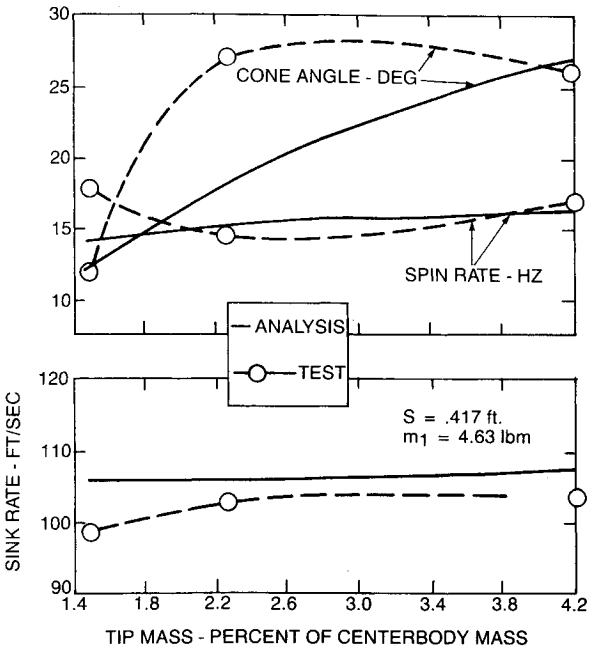

Fig. 10 Comparison of analysis and test, 5 lb model, 5 in. span.

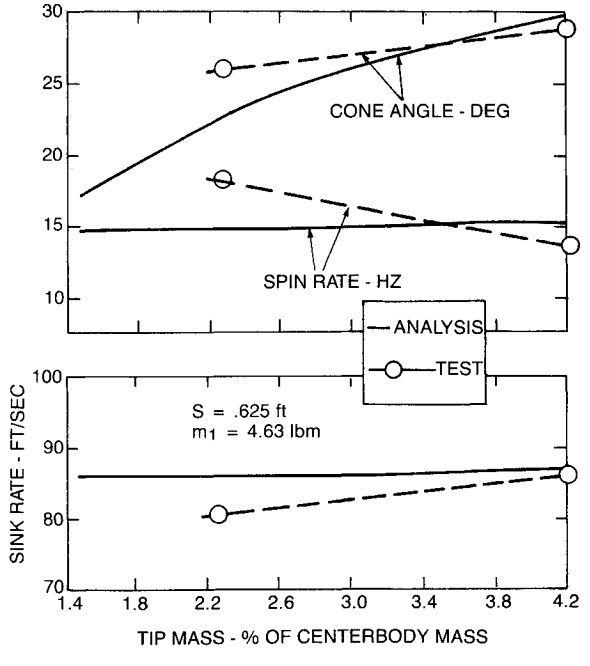

Fig. 11 Comparison of analysis and test, 5 lb model, 7.5 in. span.

In summary, the overall agreement between analysis and test results is reasonably good. With regard to those instances where there are substantial differences in one or more of the descent characteristics, it should be noted that certain details of the model designs, such as the type of attachment of the wing root to the centerbody and the retention of the tip mass, are not taken into account with the idealized model of the samara wing. These details presumably control, to some extent, the path of the tensile load between the centerbody and the tip mass, which in turn can affect wing torsional response and aerodynamic loading. Refinement of the analytic model, possibly by changing the number and/or configuration of the elastic restraints to replicate specific model designs, may improve quantitative agreement between analysis and test.

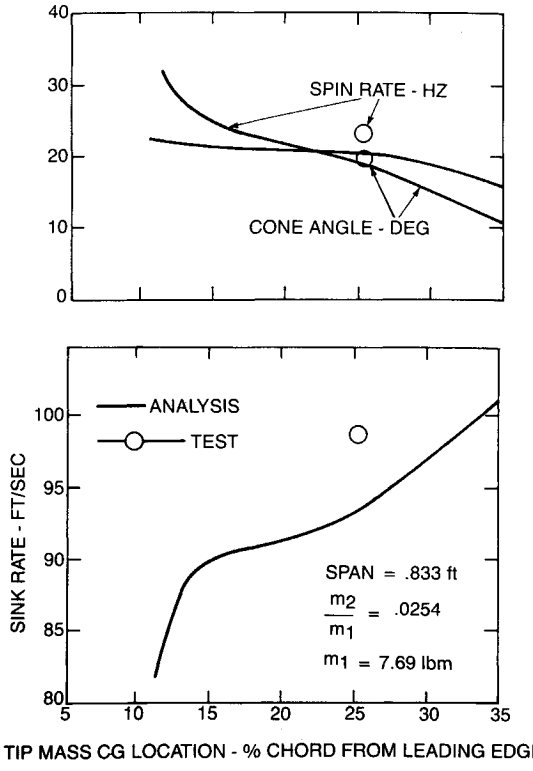

Fig. 12 Comparison of analysis and test, 8 lb model, 10 in. span.

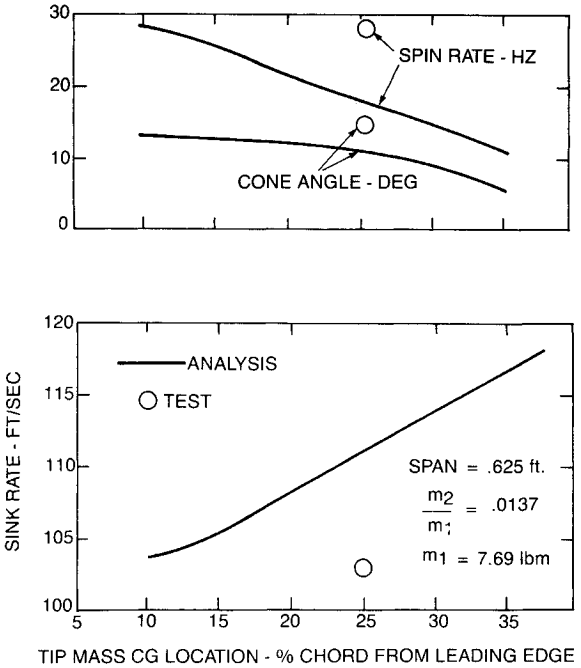

Fig. 13 Comparison of analysis and test, 8 lb model, 7.5 in. span.

Application of the Analysis Method for Samara-Wing Design

The analysis method provides a tool for developing samara-wing designs for specified descent characteristics and centerbody geometry and inertial properties. Specifically, by systematically varying the three primary wing parameters—span, tip mass, and tip mass c.g. location—a matrix of solutions can be generated, from which the required descent characteristics can be extracted by interpolation. This procedure was used to effect design solutions for two hypothetical submunition designs.

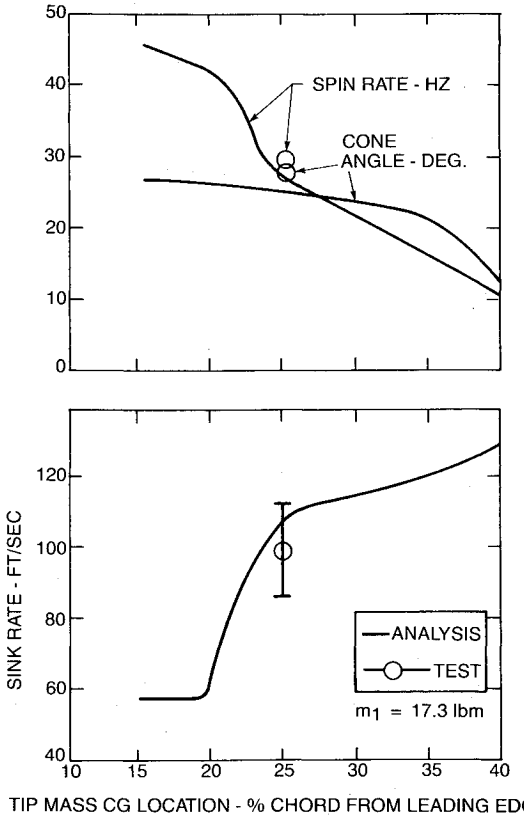

Fig. 14 Comparison of analysis and test, 17 lb model.

Design goals selected for the descent parameters are as follows: 100 ft/s sink rate, 25 Hz spin rate, and 30 deg cone angle.

Two different centerbody configurations were considered, one weighing 8 lb and the other 14 lb. Wing chords were selected to be 3 in. for the smaller submunition and 3.6 in. for the larger one. Design solutions were obtained by systematically varing wing span, with parametric variations first in tip mass and then in tip mass c.g. location, until all three descent parameters approximately matched the desired values. The parameters for the two design solutions are listed in Table 2.

Conclusions

1) Solutions for steady vertical descent in lunar rotation of a submunition with a samara-wing decelerator are generally in good agreement with test results for a wide range of model parameters.

Table 2 Configurations for design analysis and descent characteristics of design solutions

Parameter	Values Design A	Design B
Centerbody		
m_1, lbm	8.0	14.0
Diameter, in.	5.0	5.8
Height, in.	5.0	5.0
I_{x1}, I_{y1}, lb·in.^{2}	26.8	74.7
I_{z1}, lb·in.^{2}	28.2	78.4
Samara wing		
Span, in.	10.77	7.91
Chord, in.	3.00	3.60
m_2, lbm	0.100	0.119
Tip mass c.g., % chord	12.4	8.7
Descent characteristics		
Sink, rate, ft/s	100.0	100.0
Spin rate, Hz	25.0	25.0
Cone angle, deg	30.0	30.1

2) Differences between analysis and test results can be attributable in some cases to difficulties in achieving steady-state test conditions. In other cases, effects of wing and tip weight attachments on wing torsional response may not be adequately modeled.

3) Samara-wing designs can be readily generated using the analysis method by parametrically varying span, tip mass, and tip mass center-of-gravity location to effect required descent characteristics.

References

[1]Dashcund, D., "IRAAM Wind Tunnel Test—Task III," Avco Systems Div., Wilmington, MA, Rept. AVSD-0343-83-RR, Aug. 1983.

[2]"Final Report—Defense Suppression Submunition Program," Avco Systems Textron, Wilmington, MA, to be published.

[3]Kline, R. and Koenig, W., "Samara Type Decelerators," AIAA Paper 84-0807, April 1984.

[4]Crimi, P., "Analytic Modeling of a Samara-Wing Decelerator," AIAA Paper 86-2439, Oct. 1986.

[5]Hoerner, S., *Fluid-Dynamic Drag*, published by author, Brick Town, NJ, 1965, pp. 3-12.

[6]Darling, J., "Handbook of Blunt-Body Aerodynamics, Vol. I-Static Stability," Naval Ordnance Laboratories, Tech Rept. NOLTR 73-225, Dec. 1973.

[7]Gessow, A. and Myers, G., *Aerodynamics of the Helicopter*, Ungar, New York, 1967, pp. 126-130.

[8]Critzos, C., Heyson, H., and Boswinkle, R., "Aerodynamic Characteristics of NACA 0012 Airfoil Section at Angles of Attack from 0° to 180°," NACA TN 3361, Jan. 1955.